Predicting Crystal Structures and Properties of Matter at Extreme Conditions via Quantum Mechanics: The Pressure is On

Journal:	*Physical Chemistry Chemical Physics*
Manuscript ID:	CP-PER-10-2014-004445.R1
Article Type:	Perspective
Date Submitted by the Author:	05-Nov-2014
Complete List of Authors:	Zurek, Eva; SUNY at Buffalo, Chemistry Grochala, Wojciech; University of Warsaw, Department of Chemistry

Physical Chemistry Chemical Physics
CREATED USING THE RSC LaTeX PCCP ARTICLE TEMPLATE – SEE www.rsc.org/electronicfiles FOR DETAILS
ARTICLE TYPE www. rsc.org/xxxxxx | XXXXXXXX

Predicting Crystal Structures and Properties of Matter at Extreme Conditions via Quantum Mechanics: The Pressure is On

Eva Zurek[*a] **and Wojciech Grochala**[*b]

Received Xth XXXXXXXXXX 20XX, Accepted Xth XXXXXXXXX 20XX
First published on the web Xth XXXXXXXXXX 200X
DOI: 10.1039/b000000x

Experimental studies of compressed matter are now routinely conducted at pressures exceeding 1 mln atm (100 GPa) and occasionally they even surpass 10 mln atm (1 TPa). The structure and properties of solids that have been so significantly squeezed differ considerably from those know at ambient pressures (1 atm), often times leading to new and unexpected physics. Chemical reactivity is also substantially altered in the extreme pressure regime. In this feature paper we describe how synergy between theory and experiment can pave the road towards new experimental discoveries. Because chemical rules-of-thumb established at 1 atm often fail to predict the structures of solids under high pressure, automated crystal structure prediction (CSP) methods have been increasingly employed. After outlining the most important CSP techniques, we showcase a few examples from the recent literature that exemplify just how useful theory can be as an aid in the interpretation of experimental data, describe exciting theoretical predictions that are guiding experiment, and discuss when the computational methods that are currently routinely employed fail. Finally, we forecast important problems that will be targeted by theory as theoretical methods undergo rapid development, along with the simultaneous increase of computational power.

1 Introduction

High pressure can be used to access new stoichiometries, crystal structures, and novel electronic and magnetic states of matter[1–9]. For example, in 2004 experiments revealed that when elemental nitrogen is subject to temperatures above 2000 K and pressures exceeding 110 GPa, it forms the insulating single-bonded cubic-gauche phase[10]. Remarkably, this phase was predicted theoretically[11] over a decade before its experimental verification. Similarly, in 2009 it was experimentally shown that at ∼200 GPa the 'simple' metal sodium becomes insulating with a band gap of ∼1.3 eV[12]. The theoretical prediction[13] that the pressure-induced overlap of the Na $2p$ cores will push the valence electrons into the interstitial regions rendering sodium insulating preceded experiment by about 8 years. In some cases the modification of the electronic structure of a system under pressure may even result in superconductivity: eg. at least 23 elements become superconducting when squeezed, including oxygen, cesium, iodine and iron[14]. And, 30 more elements have their superconducting transition temperature, T_c, affected by pressure[15].

The pressure variable can also be employed in chemical synthesis to access phases that are metastable at ambient conditions. A famous example is diamond, which is less stable than graphite at 1 atm and 298 K[18], forming within the Earth at pressures of 4.5-6 GPa. But because the barriers to decomposition are so high (as a result of the strong C-C sp^3-bonds), diamond does not convert to graphite when the pressure is released. And pressure may also coerce elements that do not

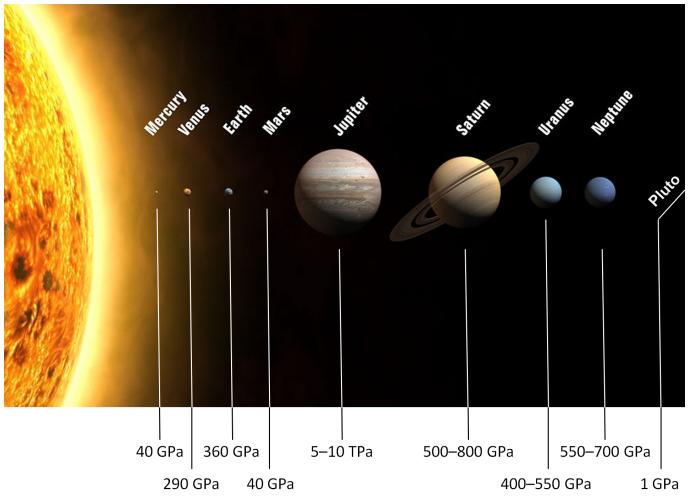

Fig. 1 The pressures of the planetary cores in our solar system. In the universe pressure spans over an astounding sixty orders of magnitude, from the pressure in intergalactic space (10^{-32} atm) to the center of a neutron star (10^{32} atm). Those reached so far in the laboratory range between ca. $6.7\text{x}10^{-20}$ atm[16] and $5\text{x}10^{7}$ atm[17].

[a] *Department of Chemistry, State University of New York at Buffalo, Buffalo, New York 14260-3000. Fax: 1-716-645-6963; E-mail:ezurek@buffalo.edu.*
[b] *Center for New Technologies, University of Warsaw, Żwirki i Wigury 93, 02089 Warsaw, Poland. Fax: (+) 48 22 55 40 801; E-mail:w.grochala@cent.uw.edu.pl.*

usually form compounds to do so, or to mix in unique proportions. One example is $NaCl_3$, which has recently been synthesized at 55-60 GPa in a laser-heated diamond anvil cell (DAC)[19]. These are just a few examples of how pressure can be utilized to create materials with unusual electronic structures, properties, and stoichiometries.

Pressure is not only a key variable within chemistry and materials science, indeed it is exceedingly important to earth and planetary science (the pressure at the center of the Earth is ∼350 GPa, and the pressures in the interiors of giant planets may fall in the TPa range, see Fig. 1), and extreme situations such as nuclear explosions. In a number of very fruitful and long-lasting efforts experimentalists have managed to create (p,T) conditions typical for the interiors of small and medium planets[17,20], and they have been able to systematically study many 'simple' chemical systems, including most of the elements[21], as well as selected binary and higher compositions under pressure. At the same time, the theoretical understanding of matter subject to high pressures has steadily advanced.

The experimental high-pressure community relies on theory to: (i) aid in structural characterization, (ii) confirm the electronic structure and properties of a material once its structure is known, and (iii) predict novel compounds or states of matter as targets for synthesis. There is substantial synergy between experiment and theory, and this feedback loop between the two communities is of utmost importance in order to advance the field. In this account we will focus on the role of theoretical tools for investigating the crystal structures, stability, and electronic and magnetic properties of matter at high pressures.

2 Methods for Structure Prediction

Crystal structure prediction (CSP) is a global optimization problem, where the atomic positions and unit cell parameters are the variables, and the multidimensional potential (free) energy surface (PES) represents the function to be minimized. The only way to guarantee that the global minimum in the PES has been found is by performing an exhaustive search over all local minima. But since the number of local minima grows exponentially with system size[22], such a task is unfeasible for all but the simplest systems. So how do we predict the structures of stable and metastable phases under pressure[23]?

The simplest strategy is to employ structural analogies, such as phenomenological structure maps[24], or data-mining of known structures[25]. Unfortunately, the scientific community has not yet collected sufficient high-quality experimental and computational results to construct a high-pressure structure database, and chemical trends obtained at 1 atm are likely to provide little predictive power under conditions of extreme pressure. They may, however, be used as starting points for generating plausible structures, as described in Sec. 2.1.

Another option is to employ algorithms designed to solve global optimization problems. Such methods have been used extensively in diverse fields including engineering (electrical circuit design) and biology (protein folding). They have subsequently been adapted towards the structure search problem, and a couple of classic applications include predictions of the structures of the Li_3RuO_4 crystal lattice[26] and fullerene clusters[27]. In these first studies the energy evaluations were carried out using empirical potentials or force fields. Luckily, the amazing advances in computational power and development of user-friendly program packages have made it practical to interface structure prediction algorithms with first-principles quantum mechanical (QM) programs in the last decade. As with structural databases, most force fields have been developed for systems at 1 atm, so for compressed solids it is important to employ global optimization techniques in conjunction with QM-based methods for energy evaluations and geometry optimizations (or suitably parameterized force fields).

In Sec. 2.1- Sec. 2.7 we briefly describe a number of algorithms commonly used to predict the structures of extended systems under pressure. Often times these methods are employed to find the global minimum, however in certain circumstances it may be useful to locate low enthalpy local-minima and/or minima subject to a set of certain constraints (i.e. intermolecular connectives) instead. For example, many unique metastable phases of carbon have been predicted under pressure[28,29]. Generally speaking basin hopping, minima hopping, metadynamics and simulated annealing are best used to find local minima that are structurally similar to the initial starting guess. Random structure searches, evolutionary algorithms and the particle swarm optimization technique perform a more thorough exploration of the PES, so they are the methods of choice when the structure is wholly unknown. In addition to structure prediction, the first set of techniques can also be used to obtain transition barriers whereas the second set cannot. Hybrid approaches that use either a mixture of computational strategies (i.e. evolutionary metadynamics[30]) or computational approaches that are guided in part by experimental results[31], have also been proposed. In this paragraph we list some of the challenges facing the CSP field today. Due to the stochastic nature of global optimization algorithms, they are difficult to benchmark. The success rate of a given method and parameter set can often only be determined via carrying out statistics on a large number of runs. This may become computationally unfeasible in conjunction with first-principles energy evaluations and geometry optimizations. Because the calculation of vibrational frequencies is computationally expensive, most applications attempt to find a subset of important structures at 0 K, and only in some cases are their free energies compared. Since the crystal with the lowest free energy (for a given temperature and pressure) may have very different structural features than the global minimum at 0 K,

this approach may fail. In principle metadynamics or molecular dynamics can be employed to predict structures at finite temperatures, but in practice long simulation times may be required to adequately sample the free energy landscape.

2.1 Following Imaginary Phonons

A geometry optimization yields a stationary point on the PES, which is a structure whose first derivative of the energy with respect to the nuclear coordinates is (close to) zero. To determine whether this geometry corresponds to a minimum on the PES, second derivatives of the energy (which are proportional to the square root of the vibrational frequency) must be calculated. If all of the frequencies are real, the geometry corresponds to a minimum. Because negative curvatures of the PES give rise to imaginary frequencies, they are indicative of structural instabilities. One valuable modification of the "structure maps" approach begins by calculating the full phonon spectrum for each prototypical structure considered in order to detect imaginary phonon branches. In the next step, the crystal structure is distorted along the normal vector of an imaginary phonon (in most cases its symmetry is lowered as compared to the parent structure), and the geometry is relaxed again. If more imaginary phonons are detected, more optimizations are carried out in order to find the structure with the most negative free energy. It is the experience of one of these authors (WG) that very often the lowest energy structure is found when following imaginary phonons not originating at the zone center, but rather off-center. This implies that a distortion leading to a decrease in the energy may be described only using a (sometimes quite large) supercell, and it results in a lowering of the symmetry. Obviously, this iterative procedure may be applied for structures both at ambient and at elevated (or even formally negative) external pressures.

The usefulness of this approach has been demonstrated recently for understanding the complex crystal structures of late transition metal monoxides (LTM MOs)[32]. It has been shown that all LTM MOs that do not crystallize in the rock salt type structure (those of Pd, Pt, Cu, Ag, Hg) in fact originate from this structure and the same imaginary phonon mode[32]. All complex orbital-ordering patterns detected for LTM MOs couple to this doubly degenerate acoustic mode with the irreducible representation L3, in the undistorted rock salt structures of the respective LTM MO. This mode, located at the L-point $(\frac{1}{2},\frac{1}{2},\frac{1}{2})$ in the Brillouin zone, attains the largest imaginary frequency in all cases, while in CuO and HgO it is the only imaginary mode found (Fig. 2)[32]. While the method of following imaginary phonons requires calculation of the entire phonon spectrum, and as such it is certainly time consuming, it has the great advantage of (i) making links between seemingly unrelated crystal structures, and (ii) understanding complex crystal structures as originating from certain electronically driven distortions for much simpler prototype structures. In this way, a great number of crystal structures may systematically be analyzed, linked, categorized into families, and their details explained. Moreover, this method (iii) always terminates the quest for crystal structures at dynamically (i.e. phonon) stable structures, i.e. at local minima, albeit without the warranty that the global minimum has been found. Similar studies may of course be performed as a function of the external pressure, e.g. to determine at which pressure conditions the imaginary phonons would entirely disappear, or new imaginary phonons would appear.

The above-mentioned method has been successfully applied in the past for predicting the crystal structure of compressed polymeric silane at elevated pressures[33]. SiH_4 has been intensely studied by the high pressure community for over a decade now due to the prediction that H-rich systems with "chemically precompressed hydrogen" might become metallic – and also superconducting – at much lower pressures than hydrogen itself[34]. The first theoretical study of compressed silane[35] predicted its polymerization and subsequent metalization at experimentally achievable pressures. Subsequent DAC experiments suggested that upon compression above

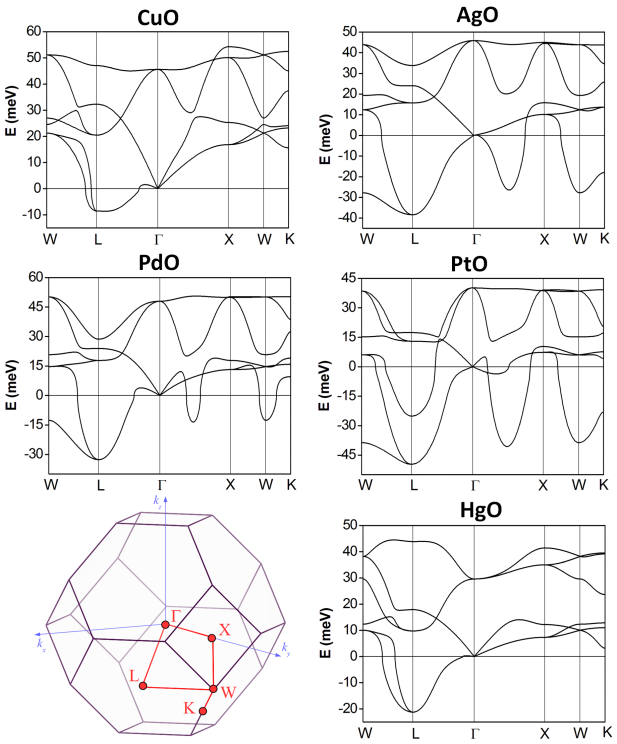

Fig. 2 Phonon dispersion curves calculated at the DFT (PBEsol) level for the LTM oxides in $Fm\bar{3}m$ cells. The first Brillouin zone of the NaCl-type cell is also shown. Reproduced with permission from Ref.[32].

26.5 GPa silane forms a polymeric[36] phase VI, whose crystal structure has not yet been solved unambiguously[37]. It turns out that the imaginary phonon-guided DFT calculations for the $I\bar{4}2d$ cell (Fig. 3) led to a polymeric $Fdd2$ structure, which is the lowest-enthalpy polymorph of SiH_4 above 26.8 GPa, and which most probably corresponds to the experimentally observed polymeric phase[33]. The phonon dispersion for the $I\bar{4}2d$ polymorph calculated for $P = 15$ GPa indicates that this system is dynamically unstable. Two imaginary vibrations appear at the Γ-point (one of $B1$ symmetry and wavenumber $143i$ cm^{-1}, the second of $B2$ symmetry and wavenumber $945i$ cm^{-1}). The distortion introduced by the $B2$ mode (which leads to a steeper PES than that for the $B1$ mode) results in the transformation of the SiH_4 tetrahedron into a butterfly with a simultaneous introduction of two additional hydrogen atoms from the neighboring SiH_4 molecule into the first coordination sphere of silicon (Fig. 3). The resulting $Fdd2$ structure contains an extended polymeric Si-H network and it becomes stable with respect to the lowest-enthalpy molecular polymorph of SiH_4 at pressures exceeding 26.8 GPa. Notice the excellent agreement of the experimentally observed (26.5 GPa) and theoretically predicted (26.8 GPa) pressure of the phase transition, which is connected with the polymerization of silane. Moreover, similar calculations for other phases proposed in numerous theoretical studies have shown that the seemingly simple SiH_4 system has a very complicated PES, since all of the previously examined structures exhibit phonon instabilities for at least one pressure point from the range 15-125 GPa. In other words, they did not constitute local minima within certain pressure ranges. This example shows the crucial role of calculating the phonon dispersion of experimentally relevant crystal structures.

Another nice example of how the "following imaginary phonon modes" approach works in predicting crystal structures – this time of a hitherto unknown compound – is provided by AuF[38,39]. This elusive compound has not yet been prepared in the solid state although its silver(I) analogue is well known. A theoretical study[39] showed that the lowest-enthalpy orthorhombic (O1) structure may be obtained from the NaCl-prototype by a sequence of phonon distortions (Fig. 4), and it's enthalpy at 5 GPa is lower than that of the previously considered AuCl-type and AuI-type structures[40]. Moreover, the previously suggested structures proved not to be local minima at all, i.e. they exhibited imaginary frequencies for at least one pressure point in the 5-15 GPa range. In the same study the tetragonal T3 structure[38], which is also NaCl-related, was found to be adopted by AuF at pressures higher than 20 GPa, and the origins of difficulties in obtaining AuF were pointed out (even the O1 structure has proven to be thermodynamically unstable to disproportionation despite its dynamic stability). The case of AuF has also illustrated that it is very didactic to begin the imaginary phonon quest with high-symmetry prototypical structures, such as NaCl- or CsCl-type. Starting with these high-energy "unrealistic" ionic structures will by necessity result in many substantially imaginary modes in solids presumed to exhibit covalent bonding. Following these modes may ultimately lead towards the lowest energy structure.

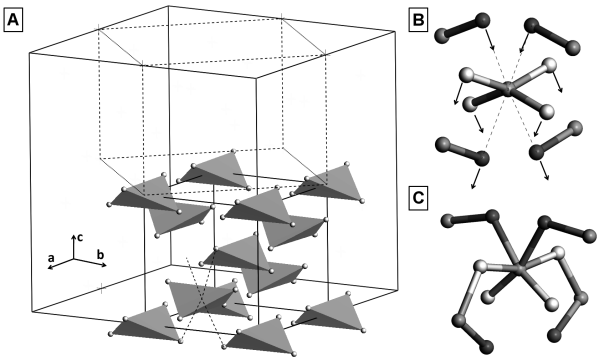

Fig. 3 (A) The crystal structure of $I\bar{4}2d$ SiH_4 at 15 GPa (the small black box represents the unit cell, and the large one illustrates the $2 \times 2 \times 2$ supercell used for calculating the phonon dispersion curves). Tetrahedra formed by four Si-H bonds are marked in gray, dashed lines mark additional H···Si contacts. The unit cell of the structure obtained after following the imaginary B_2 mode is marked with dashed lines. (B) Movement of atoms in the B_2 vibration (gray/white balls – Si/H from the 1st coordination sphere of Si, dark gray balls – H from neighboring SiH_4 tetrahedra). (C) View of the corner-linked distorted SiH_6 octahedron present in the polymeric $Fdd2$ structure. Reproduced with permission from Ref.[33].

In a very similar fashion the crystal structures of the XeAuF adduct have been predicted at ambient and elevated pressures by theory for the first time[41]. One might anticipate that in the near future the imaginary-phonon-based structure quest will be made fully automatic via constructing programs linking relevant computational suites such as PHONON[42] and VASP[43,44], in a similar fashion as the other modern structure-prediction tools described in the sections below.

2.2 Random Searching

Perhaps the simplest way to automatically generate candidate structures is by randomly choosing their atomic coordinates and lattice vectors. But, since completely random choices are likely to yield numerous high energy structures, it is a good idea to impose constraints, based on chemical principles, that limit the search to reasonable regions of the PES. Two seemingly trivial, but extremely useful, constraints are the unit cell volumes and interatomic distance limitations. The unit cell parameters and their likely symmetries can further bias the search space to chemically relevant regions, particularly if experimental data is available. Enforcing connectives between

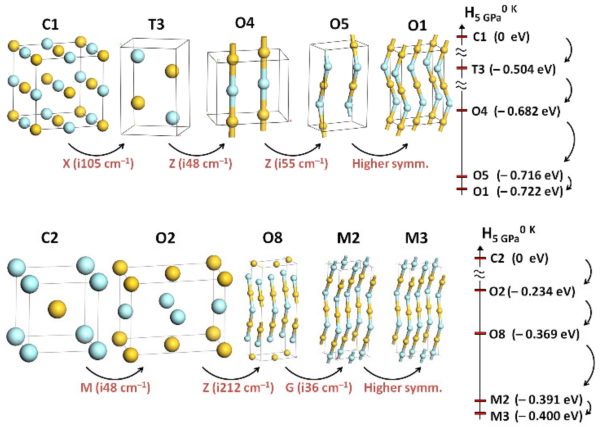

Fig. 4 Selected cubic, tetragonal and orthorhombic crystal structures of Au(I)F considered theoretically[38]. Top: from left to right: a parent ionic $Fm\bar{3}m$ NaCl-type (C1) structure, and four others derived from phonon instabilities: $P4/nmm$ (T3); $Pmmn$ (O4); $Pnma$ (O5); $Cmcm$ (O1) – obtained from O5 after symmetry recognition with a restrictive threshold and reoptimization. Bottom: from left to right: a parent ionic $Pm\bar{3}m$ CsCl-type (C2) structure, and four others derived from phonon instabilities: $Cmmm$ (O2); $Amm2$ (O8); Cm (M2); $C2/m$ (M3) – obtained from M2 after symmetrization. Arrows indicate the relationship between the parent and the derived structures, and also show which imaginary phonon mode was followed. Nomenclature of the polymorphs is consistent with that used in Ref.[39]. Light/dark balls represent gold/fluorine atoms. Reproduced with permission from Ref.[38].

atoms, by using molecules or clusters as building blocks, can be exceedingly useful for predicting the structures of molecular solids or phases likely to contain unique structural motifs such as tetrahedra or icosahedra. In a random search, each structure that is generated is optimized to the nearest local minimum; this procedure is schematically represented in Fig. 5. Enforcing chemically reasonable constraints speeds up each local relaxation and dramatically increases the success rate. The drawback of purely random searches is that they do not learn from their history, so they cannot zoom in on particularly promising regions of the PES as the search progresses. The methods described in Sec. 2.3 - Sec. 2.7 often begin with calculations on a randomly generated set of crystalline lattices.

Pickard and Needs have developed a particularly powerful version of this technique, the *ab initio* random structure searching (AIRSS) method[45,46]. The structures generated by AIRSS can be subject to a variety of constraints. In addition, AIRSS allows stable structures to be mutated via random atomic displacements and random unit cell deformations. This procedure, referred to as 'shaking', allows the algorithm to learn as the search progresses. Random searches have been employed to predict the structures of a plethora of compressed

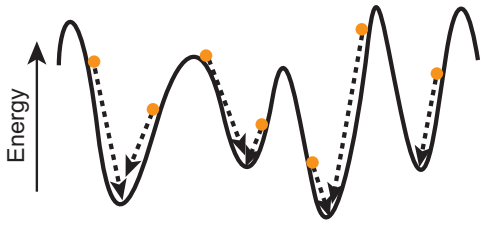

Fig. 5 A schematic illustration of the random structure searching method in a 1-dimensional PES. The dots represent structures, and the dashed black arrows local optimizations.

solids including LiBe[47], hydrogen[48], lithium[49,50], ammonia[51], hydrogen-oxygen mixtures[52], among many others.

2.3 Simulated Annealing

One of the simplest methods that explores the PES via overcoming energy barriers is simulated annealing[53]. The inspiration for this algorithm originated from the metallurgical process of heating a substance followed by cooling, until crystallization occurs in a controlled fashion. Simulated annealing has been applied to many global optimization problems. One well-known example is the traveling salesman problem, which aims to find the shortest route a salesman takes so that he passes once through each city on a list prior to coming home.

A simulated annealing search begins by calculating the energy of a (randomly selected or user defined) ensemble of atoms. The atoms are perturbed via random displacements, permutations of atoms of different types, or changing the parameters of the unit cell. The energy of the new configuration is calculated, and the structure is accepted or rejected based upon the probability, $P = \exp(-\Delta E/k_B T)$, where ΔE is the energy difference between the two configurations, k_B is the Boltzmann constant, and T is the simulation temperature. A random number, ε, between 0 and 1 is chosen, and if $\varepsilon < P$ the new structure is accepted. If the configuration is rejected, a new one is created and the procedure is repeated. The algorithm used to accept or reject structures corresponds to the well known Monte-Carlo method of Metropolis. The simulation begins at high temperatures, so that most configurations are accepted. In such a way, the initial structure starts to 'melt'. The temperature is gradually decreased during the simulation, with fewer high energy structures being accepted as the run progresses. This mimics the physical annealing process. Finally, the temperature is set to 0 K, at which point only downhill steps are accepted and the system 'freezes' into the nearest minimum.

One of the drawbacks of simulated annealing is that the high temperature PES may not coincide with the low temperature one, so the search may become stuck in unfavorable regions of the PES upon cooling. Annealing schedules that raise the

temperature temporarily during the course of the run can be used in an attempt to overcome this problem. It is important to choose the magnitude of the random mutation judiciously – it should be large enough to escape local minima, but small enough to enable learning. And it may be necessary to carry out multiple annealing runs if a good starting structure is not known. Doll, Schön, Jansen and co-workers have successfully used simulated annealing to predict the structures of a wide variety of inorganic crystals including lead sulfide[54], lithium[55] and calcium carbide[56].

2.4 Basin and Minima Hopping

Basin hopping[57] and minima hopping[58] also explore the PES by overcoming energy barriers. Even though basin hopping uses a Monte-Carlo procedure to determine whether or not newly created structures are accepted or rejected, it differs from simulated annealing in a number of important ways. Specifically, in basin hopping (i) the initial configurations are optimized to the nearest local minimum at each step, (ii) the energies of the relaxed structures are employed to determine the probability for acceptance, (iii) the same temperature can be maintained during the course of the entire run. Because every configuration that falls within a single basin in the PES ultimately optimizes to the same local minimum, it is often said that the algorithm transforms the PES into a series of interpenetrating step functions (see Fig. 6(a)). If the starting configuration is sufficiently perturbed, then the algorithm can hop from the minimum of one basin to the next. But, perturbations that are too aggressive do not allow the algorithm to learn during the course of the run, causing it to behave basically like a random search. Drawbacks of the method include the difficulty associated with determining an optimal temperature for the run, and the fact that there is no penalty associated with re-exploration of an already visited basin. Basin hopping has been used extensively to predict the structures of finite clusters[57], but we are not aware of an application towards extended systems under pressure.

The minima hopping method was introduced by Goedecker to overcome some of the problems associated with basin hopping[58]. Minima hopping is not a Monte-Carlo method. Because it uses molecular dynamics (MD) to explore the PES instead, a temperature that controls the acceptance/rejection ratio need not be chosen. Each structure is optimized to the nearest local minimum. The energy of the current configuration is compared with that of the new structure, and the variable determining whether or not this configuration is accepted, E_{diff} see Fig. 6(b), is continually adjusted so that the acceptance ratio constantly remains fixed at 50%. The kinetic energy used in the MD step is adjusted so that about half of the time the system can surpass a barrier and enter a new basin. The kinetic energy may also be raised in order to discourage

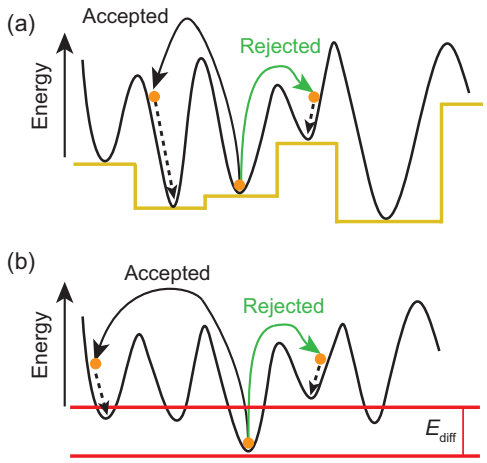

Fig. 6 Same as Fig. 5, but for (a) basin hopping and (b) minima hopping.

revisitation of previously explored minima. This method has been employed extensively to predict the structures of crystals under pressure, a few examples include disilane[59], carbon[29] and a series of alanates[60].

2.5 Metadynamics

Metadynamics[61] is an MD-based method where the forces are modified by a history dependent term. The basin that is under exploration is filled with Gaussians during the course of the simulation, resulting in the continuous lifting of the potential within the basin. Eventually, the potential becomes high enough so that the algorithm can overcome a barrier and fall into a nearby local minimum. This procedure, illustrated schematically in Fig. 7, allows the search to overcome barriers and prevents the re-exploration of already visited regions of the PES. One of the disadvantages of metadynamics is that it discourages the use of transition pathways that are shared between multiple minima. Flooding such a transition basin may prevent the global minimum from being found in a single run, so that it may be necessary to carry out a number of searches starting from different initial configurations. In addition to structure prediction, metadynamics can be used to accelerate rare events in dynamics simulations. This feature is useful for the study of structural phase transitions, mechanisms of chemical reactions, and conformational changes in solution. Metadynamics has been extensively employed to predict new structural modifications under pressure for a plethora of systems including germanium[62], calcium[49], and CO_2[63].

2.6 Particle Swarm Optimization

In a purely random search each structure that is generated is independent of the others that preceded it. Because of this,

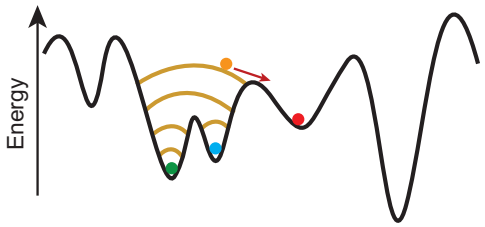

Fig. 7 Same as Fig. 5, but for metadynamics.

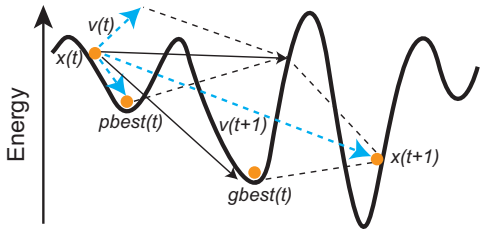

Fig. 8 Same as Fig. 5, but for the particle swarm optimization technique (PSO). See Eq. 1 and Eq. 2 for how the specified quantities (i.e. $x(t)$, $gbest(t)$) are employed to make a new structure.

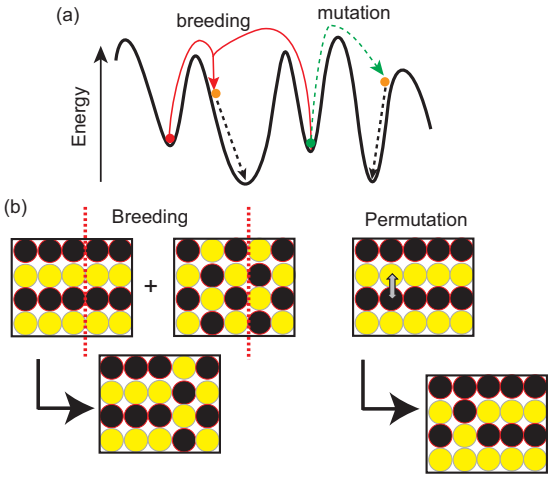

Fig. 9 (a) Same as Fig. 5, but for genetic or evolutionary algorithms. (b) Illustration of the 'breeding' (or heredity) operator, which cuts two parents using a randomly positioned plane, and splices two of the four portions into a single child (in principle two unique children can be made in this way, but typically only one child is chosen for further evolution). The 'permutation' operator acts on a single parent by interchanging the positions of two or more atoms of different types.

the algorithm is unable to learn about where the valleys (and highpoints) in the PES may be located during the course of the run. One method that is able to learn from history, and is therefore more likely to zoom in on the minima as the search progresses, is the particle-swarm optimization (PSO) technique. This global optimization method was inspired by the collective behavior (swarming) that certain types of animals, such as birds or fish, exhibit during their migration. Ma and coworkers were the first to adapt this algorithm towards structure prediction in the CALYPSO code[64,65].

As an example let us consider a flock of birds. The position of each individual bird at some instant ($x(t+1)$) is dependent upon it's former position ($x(t)$) as well as it's velocity ($v(t+1)$) as

$$x(t+1) = x(t) + v(t+1). \quad (1)$$

The velocity of the bird can be calculated via

$$v(t+1) = \omega v(t) + c_1 r_1 (pbest(t) - x(t)) + c_2 r_2 (gbest(t) - x(t)). \quad (2)$$

where $v(t)$ is the velocity at step t, $gbest(t)$ is the position of the leading bird (i.e. global minimum for a given population), ω is an inertia weight, r_1 and r_2 are random numbers, and the coefficients c_1 and c_2 are factors that illustrate how much the individual trusts its own position as opposed to that of the leader of the flock. The quantities $x(t)$ and $pbest(t)$ cannot be so easily understood in terms of the positions and movements of birds. The first term corresponds to the previous location of the structure on the PES prior to local optimization, whereas the second refers to the optimized structure. This procedure is illustrated schematically in Fig. 8. Typically, the first set of structures in the PSO algorithm is generated randomly (subject to interatomic distance, volume and symmetry constraints), followed by local optimization. Subsequent structures are created via Eqs. 1 and 2. The PSO method has been applied towards myriad high-pressure systems including calcium polyhydrides[66], cesium polyfluorides[67] and water[68].

2.7 Evolutionary Algorithms

Another set of stochastic search techniques that learn during their exploration of the PES are evolutionary/genetic algorithms (EAs/GAs)[23]. These methods attempt to find the global minimum by making use of evolutionary principles, such as survival of the fittest as well as procreation and mutation. They employ a thermodynamic quantity to determine a structure's fitness, or probability to be chosen for breeding, thereby 'evolving' towards the most stable structure. A typical workflow of an EA/GA for CSP begins with the construction of an initial generation of sensible random structures (seeding is also possible), followed by local optimization, and the creation of 'children' by combinations of two parents (breeding) or mutations of a single parent.

There is a subtle difference between GAs and EAs, even though the two terms are often used interchangeably. In a GA the structures are mapped onto a binary string and the mutation and breeding operations are carried out on this string. In an EA the evolutionary operators act on the structures in real space. Fig. 9(a) illustrates schematically the way EAs

explore the PES. Breeding combines two parents into a single child, and it is sometimes referred to as crossover, heredity or the 'cut-and-splice' operator[27]. Two parent structures are chosen, and a spatially coherent subset of each parent's atoms are selected and joined in fractional coordinate space[69], as shown in Fig. 9(b). A randomly weighted average of the parents' cell vectors are used to determine the dimensions of the child's lattice. Children can be formed via mutations of a single parent as well. One example is the permutation of two or more atoms of different types as illustrated in Fig. 9(b). Other mutations include: modification of the shape of the unit cell, displacement of atoms in the cell via a random-walk or periodic motion (such as a wave), or combinations of two or more of these operators. The structures with the lowest enthalpy have the highest probability to be chosen for procreation, in such a way ensuring that favorable traits (motifs that render the structures stable) can propagate into the next generation. In the last decade a number of groups have released EAs interfaced with first-principles periodic program packages: some of these include XTALOPT[70,71], USPEX[69,72], MAISE[73], EVO[74], GASP[75], as well as algorithms by Zunger[76,77], Abraham and Probert[78], Fadda[79], and the 'adaptive-GA' of Wentzcovitch et al.[80].

A plethora of studies have used evolutionary algorithms to predict the structures of compressed phases. A select handful of these include the polyhydride and subhydride phases[81–89] described in Sec. 6, lithium hydroxide (LiOH)[90] and water[91] up to TPa pressures , and binary and ternary phases containing the light elements Li, Be and B[92–96].

3 Accurate Reproduction of Experimental Results

Accurate reproduction of experimental observations is the most fundamental feature of reliable theoretical calculations. In this section we describe two important recent cases where theory has been able to reproduce features observed in experiment, and helped to rationalize the results obtained.

The first example is that of compressed hydrogen. Metallic hydrogen has long been sought[97], and it is often referred to as the 'Holy Grail' of high pressure science. Recent experiments revealed that molecular hydrogen transforms at room temperature (298 K) and pressures of 260-270 GPa to a highly electrically conductive state[98]. A subsequent experimental study confirmed the existence of a new phase in this region of the P/T phase diagram and provided a set of independent Raman spectra[99]. A theoretical study[100] carried out after these experiments were performed found novel non-classical phases of hydrogen consisting of alternate layers of strongly bonded molecules and weakly bonded graphene-like sheets to have the lowest free energy in the experimentally relevant pressure/temperature range. The calculations showed that mixed structures are the most stable at room temperature over the pressure range of 250-295 GPa, and they are stabilized with respect to strongly bonded molecular phases by the presence of lower frequency vibrational modes arising from the graphene-like sheets. Thus, theory has been able to rationalize experimental findings and provide likely candidate structures for the newly discovered so-called Phase IV of hydrogen.

Another case where theory and experiment have nicely converged is provided by a recent mixed experimental-theoretical study of the Na/Cl phase diagram under pressure[19]. At least two stable novel stoichiometries, Na_3Cl and $NaCl_3$, were synthesized, and theory seems to have inspired the experimental investigation. In particular, evolutionary algorithms were able to predict stable structures whose computed X-ray powder patterns could be compared to experimental data. Although these stoichiometries are not unique (it has long been known that most alkali metals and alkali halides are miscible in a very broad composition range in the liquid state[101,102], and both sub- and polyhalides are extremely common in the chemistry of halogens), they nonetheless constitute a valuable contribution to the understanding of the Na/Cl phase diagram[103].

4 Reproducing Lattice Dynamics

Lattice dynamics are an important physical property of every solid state system. Translations and rotations are usually frozen in solids, especially at low temperatures, and they transform into acoustic phonons and hindered rotations (librations), respectively[104]. Thus, lattice oscillations of solids determine many of their key thermodynamic parameters, such as the heat capacity and the entropic contribution to the Gibbs free energy. Moreover, the vibrational spectrum of a solid is – just like for molecular systems – a fingerprint of each chemical composition and every polymorphic form at a given composition, and as such it has enormous analytical value. This is of particular importance for DAC experiments where chemistry is usually difficult to control: it is nearly impossible to fix the ratio of substrates in a two-phase system, to suppress their tendency to decompose or amorphize, and the reactivity of loaded material(s) towards diamond and the gasket must sometimes be taken into account etc. Furthermore, analysis of the vibrational spectrum may help to understand chemical bonding in solids and the nature of phase transitions (order-disorder, polymerization, etc.) even if solving the crystal structure is problematic. Indeed, Raman scattering (and sometimes also infrared absorption) spectroscopy is routinely used to analyze samples compressed inside a DAC. Thus, theoretical calculations of phonon spectra may be used not only to help assess the chemical identity and type of polymorph observed experimentally, but in some cases (such as those described in Sec. 5.1 and Sec. 5.2) they may also suggest the presence of imag-

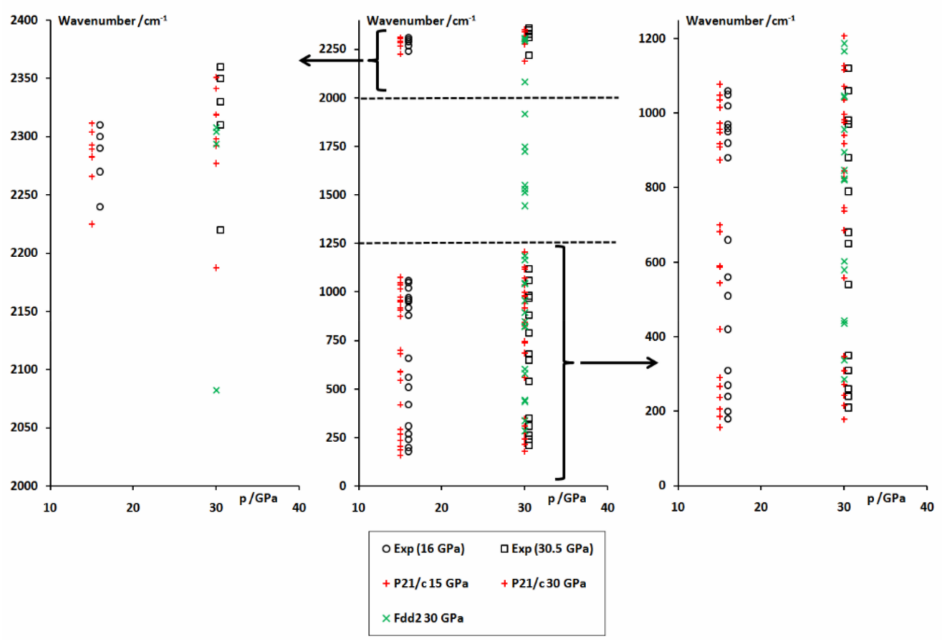

Fig. 10 Comparison of the observed (open symbols)[37] and calculated (red and green crosses)[33] Raman bands (cm^{-1}) of SiH_4 at 15 and 30 GPa (the DFT result is for 15 GPa and not 16 GPa). Note that at 16 GPa the experimental spectrum corresponds to the pure $P2_1/c$ phase, whereas at 30 GPa it corresponds to a mixture of the $P2_1/c$ and $Fdd2$ phases. Two spectral regions: (left) Si-H stretching (2100-2400 cm^{-1}) and (right) Si-H deformation and lattice modes (0-1200 cm^{-1}) are shown separately. The spectral region in which the bending and stretching of the Si-H-Si bridges in $Fdd2$ should be observed (1400-2000 cm^{-1}) was not presented in Ref.[5]. Note that the wavenumbers of the DFT-calculated modes are slightly underestimated, as typical for DFT. This is why scaling factors of 1.015 and 1.050 were applied for the stiff Si-H stretching vibrons and for all remaining modes, respectively. For group theory labels of various modes please refer to the electronic supplement of Ref.[33]. Reproduced with permission from Ref.[33].

inary phonons, which always calls for the reinterpretation of experimental results.

The usefulness of computational phonon analysis will be illustrated here as exemplified by the case of compressed silane. Because vibrations of hydrogen-element bonds usually have large frequencies, it is typically assumed that zero-point energy corrections to the total energy are large for hydrogen-containing systems such as silane. Indeed, calculations indicate that at room temperature the differences in the vibrational and entropic contributions to the Gibbs free energy of different SiH_4 polymorphs are of the order of 10 meV and thus they are negligible in comparison with the corresponding differences in the zero-point energy corrections, which reach up to 100 meV[33].

Another valuable result related to calculations of phonon spectra of different forms of silane is that polymerization may easily be detected by analyzing lattice oscillations. The high-pressure $Fdd2$ form of SiH_4 (occurring above 27 GPa) is polymeric with the Si atoms exhibiting a 2 + 2 + 2 coordination with two terminal Si-H bonds of 1.47 Å and four bridging ones at 1.59 and 1.65 Å at 30 GPa. In contrast, at the same pressure the (low-pressure) $P2_1/c$ structure still exhibits isolated SiH_4 units with an average Si-H bond length of 1.47 Å (a 1.2% contraction with respect to the silane molecule at ambient pressure) indicating that at 30 GPa $P2_1/c$ is still a molecular structure (the shortest intermolecular contact is 2.10 Å). This is nicely confirmed by an analysis of the phonon spectrum of this polymorph (Fig. 10). The Si-H stretching modes (2150-2300 cm^{-1}) have a small dispersion and their frequencies are well separated from those corresponding to the H-Si-H bending modes (900-1080 cm^{-1} at the Γ-point). The $Fdd2$ structure turns out to retain its polymeric framework upon decompression up to 5 GPa[33], as evidenced by the phonon dispersion curves calculated at each pressure for this structure. Apart from the stretching and bending vibrations of the terminal hydrogen atoms (with frequencies similar to those calculated for $P2_1/c$) the $Fdd2$ polytype exhibits modes in the 1400-2050 cm^{-1} region (Γ-point at 30 GPa) that are absent for $P2_1/c$. These can be assigned to the stretching (2050-1660 cm^{-1}) and bending (1500-1400 cm^{-1}) modes of the Si-H-Si polymeric bridges. Softening of the stretching modes and stiffening of the bending modes, as compared to the molecular $P2_1/c$ phase, is a clear signature of the polymeric nature of the $Fdd2$ phase, while the absence of imagi-

nary phonons at 5 GPa suggests the possibility that polymeric silane may be decompressed to near-ambient pressure.

5 An Aid to Interpreting Experimental Results

High-pressure experiments can be exceptionally challenging to carry out. It may be very difficult to determine the structure of a new phase directly (i.e. using X-ray diffraction), especially if it contains light elements. Often times structural information is inferred from the results of Raman or IR spectroscopy instead. Light elements may diffuse into the diamonds causing them to break, resulting in a costly and premature end to the experiments. The samples being analyzed can decompose, and unwanted reactions with substances comprising the experimental apparatus can occur. Measuring the properties (i.e. conductivity) of a sample within a DAC can also be quite a challenge and the results may be difficult to interpret. And the laser heating technique often used to drive reactions can result in burned diamonds if the laser beam is not aligned correctly. For these reasons a synergistic feedback loop between experiment and theory is often required to correctly interpret experimental results. Below, we summarize a few tales where theoretical scrutiny revealed discrepancies that could only be understood following a revision of the original interpretation of the experimental results.

5.1 Unintended Reactions

Ever since Ashcroft's prediction that metallic hydrogen would be a high-temperature superconductor[105], the high pressure community has been on a quest to produce this elusive state of matter. At the turn of the century it became clear that hydrogen could not be metalized in the limit of static compression at the time ($\sim$350 GPa), at least not at temperatures low enough so as to prevent hydrogen from diffusing into the diamonds[106,107]. Ashcroft speculated that hydrogen-rich systems, where the hydrogen was chemically bonded to another element, may undergo metalization at lower pressures than pure hydrogen because of "chemical precompression", and the resulting phases could also be high temperature superconductors[34].

Guided by Ashcroft's predictions, calculations were carried out on hydrogen-rich phases under pressure, focusing on silane as a candidate for high-temperature superconductivity[35]. Some of the predicted structures have already been discussed in Sec. 2.1 and are illustrated in Fig. 3. Many theoretical[37,108,109] and experimental[37,110,111] investigations of compressed silane followed suit. Experiments revealed that silane metalized at 50 GPa and became superconducting below 17 K at 96 and 120 GPa[111]. The diffraction pattern hinted that a phase with $P6_3$ symmetry was stable between 50-110 GPa and an $I4_1/a$ phase above 160 GPa[111]. However, further computations showed that the proposed $P6_3$ structure was dynamically unstable and it was not the lowest enthalpy phase[112–114]. An insulating $I4_1/a$ structure was found to be the most stable between 50-220 GPa[108,112,114]. Computations suggested that metastable structures with $Cmca$[112], $Pbcn$[114] or $P4/nbm$[113] symmetries could potentially be candidates for the metallic and superconducting phase. In short, the results of first-principles calculations could not be reconciled with the conclusions obtained from analyzing the experiments. A different interpretation was needed.

In the experiment platinum electrodes were employed to measure the conductivity of the sample. Noble metals do not form hydrides at 1 atm, so it was believed that platinum would remain inert under pressure as well. Degtyareva et al. realized that the X-ray diffraction pattern of the supposed metallic silane matched quite well with the one obtained for PtH, which was synthesized at pressures higher than 27 GPa, see Fig. 11. Therefore, these authors proposed that decomposition of silane under pressure could liberate hydrogen, which reacted with the platinum electrodes forming a hydride[115]. Calculations showed that the PtH stoichiometry was the most stable point on the Pt/H phase diagram at $\sim$100 GPa[116], and it was computed to become thermodynamically preferred over solid H_2 and Pt by 3 GPa[117]. Structure searches found an hcp[116,118] and fcc[118] phase that were nearly isoenthalpic at $\sim$100 GPa. Remarkably, the X-ray diffraction patterns and T_c between 80-160 GPa calculated for PtH[116,118,119] matched well with the experimental results for 'silane'[111]. Further work confirmed the room-temperature high-pressure synthesis of PtH above 27 GPa[119]. Thus, the iterative feedback loop between theory and experiment showed that the observations of Eremets could be explained by a very different interpretation than the one that was originally put forward. The discovery that silane decomposes under pressure releasing hydrogen, which subsequently reacts with platinum to form a superconducting noble metal hydride, presents a very nice example of the eventual convergence of experiment and theory.

Theoretical work has been instrumental in confirming the unintended and serendipitous formation of other unique chemical systems under pressure. One example includes the element tungsten, which is often used as a gasket material to seal hydrogen in DACs because of the presumed low reactivity between the two. It was therefore somewhat surprising when a hydride of tungsten was prepared[121,122], in experiments that ultimately revealed compound formation between SiH_4 and H_2[123]. Structure searches coupled with first-principles calculations showed that the WH, WH_2, WH_4 and WH_6 stoichiometries become thermodynamically and dynamically stable under pressure[122,124,125]. A WH stoichiometry with $P6_3/mmc$ symmetry was found to have the lowest enthalpy of formation between 25-150 GPa[122,124], and it's structure was consistent with the experimental X-ray diffraction peaks, which were indicative of an hcp WH phase. Further

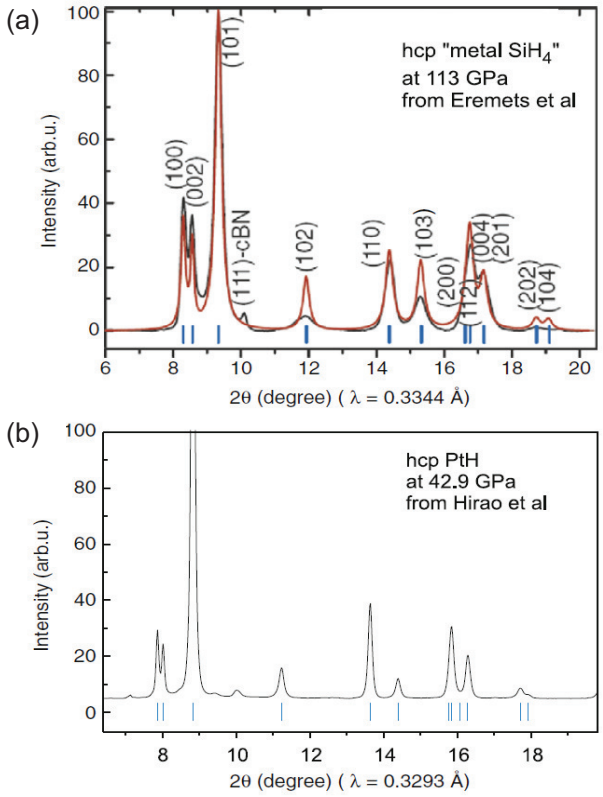

Fig. 11 Powder diffraction spectra of (a) the hcp phase of metallic silane in Ref. [111], and (b) the hcp phase of PtH from Ref. [120]. Reprinted from [115] *Solid State Commun.*, **149**, O. Degtyareva, J. E. Proctor, C. L. Guillaume, E. Gregoryanz and M. Hanfland, "Formation of Transition Metal Hydrides at High Pressures", 1583-1586, Copyright (2009), with permission from Elsevier.

experiments showed that above 50 GPa WH uptakes hydrogen such that the H:M ratio approaches $1\frac{1}{3}$ [122], but higher hydrides have not yet been synthesized.

5.2 Unknown Stoichiometries

Actually, the high pressure community should not have been surprised by the reactivity that pressure imbues to platinum (or tungsten). In 2004 Gregoryanz et al. reported the first synthesis of a binary nitride of the noble metals, platinum nitride, at 2,000 K and 45-50 GPa, which had a remarkably high bulk modulus of 372 GPa and remained metastable upon decompression [126]. Compositional profiles hinted that the synthesized phase had a PtN stoichiometry. X-ray diffraction data was consistent with both a rock-salt and zinc blend structure, but because of the large mass difference between Pt and N it was not possible to unambiguously distinguish between the two. The rock-salt structure was ruled out because it could

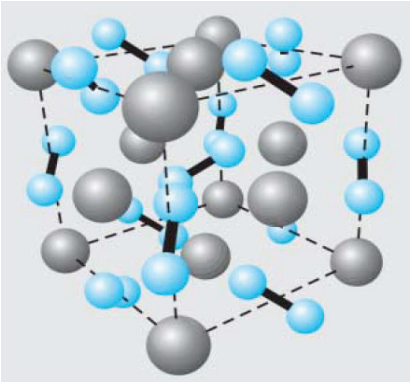

Fig. 12 The pyrite structure of PtN_2 [130]. From *Science*, **311**, J. C. Crowhurst, A. F. Goncharov, B. Sadigh, C. L. Evans, P. G. Morrall, J. L. Ferreira, A. J. Nelson, "Synthesis and Characterization of the Nitrides of Platinum and Iridium", 1275-1278, 2006. Reprinted with permission from AAAS.

not explain the observed Raman spectrum, and first-principles calculations confirmed the identity of the synthesized nitride as being PtN within the zinc blend structure [127–129].

But there were inconsistencies in the results, which suggested violation of Le Chatelier's principle, that led to a closer examination of the experimental data. This revealed that a factor of two was missed in the calculation of the bulk modulus, suggesting that the synthesized nitride could not be zinc blend PtN [131,132]. In fact, calculations on a number of different structures with a PtN stoichiometry showed that none of them could account for the experimental observations [133]. Furthermore, Yu and co-workers realized that PtN in the zinc blend structure is not mechanically stable, and proposed an alternative stable PtN_2 stoichiometry in the fluorite [134,135] and later in the pyrite [136] configurations. Crowhurst et al. carried out high pressure synthesis and characterization experiments that unambiguously confirmed that the mysterious compound was pyrite-PtN_2 [130]. Detailed first-principles computations of the enthalpies of formation, bulk moduli, X-ray and Raman spectra, electronic structure, and structural parameters of various PtN and PtN_2 crystal lattices showed that the computed observables for pyrite-PtN_2 are in excellent agreement with experiment [130,137–139]. Dronskowski and co-workers pointed out that PtN_2 should not be referred to as platinum nitride, but rather platinum diazenide (or pernitride) because the antibonding states of the N_2 molecule have been filled (N_2^{4-}) such that the N-N bond length is reminiscent of a single bond [140].

5.3 Melting Behavior

We should note that the utility of first-principles calculations is not solely restricted towards static solid phases, their structural parameters and observables. The behavior of compressed

liquid phases, as well as the determination of solid-liquid equilibria (i.e. melting lines), is also an area where computations are tremendously helpful. Melting is particularly difficult to measure experimentally. First of all, it is not easy to unambiguously pinpoint exactly when a solid melts and different criteria – including an abrupt change in the resistivity, disappearance of X-ray diffraction lines and visual observations – can be employed [141]. Measuring the temperature of a compressed sample in a DAC also affords its own set of difficulties. And finally, as outlined above, unforeseen chemical reactions between the sample and materials comprising the experimental set-up may occur.

Theoretical calculations of the melting lines face their own sets of problems including a large computational expense, potential hysteresis and overheating [142]. In addition, a number of computational (molecular dynamics based) techniques can be employed to estimate melting [143–146]. For example, there is the one-phase heat until it melts method, the two-phase or solid-liquid coexistence method, and determining the P/T conditions at which the Gibbs free energies of the liquid and the solid phases are equal. In the "Z method" a series of molecular dynamics simulations are carried out in an NVE ensemble, and a plot of the resulting P/T state gives rise to a characteristic "Z"-shaped isochore that can be used to estimate the melting temperature. Comparison of the melting lines obtained using different experimental procedures coupled with those obtained from theory help to more accurately determine the boundary between the solid and liquid phases as a function of pressure. A few computational studies calculating melting-behavior either via first-principles directly, or using interatomic potentials that have been fitted to first-principles results, include iron [147], carbon [148] and CO_2 [149] (relevant for our understanding of the conditions at the interior of the earth and other planets), hydrogen [150] and sodium [151] (whose melting temperatures *decrease* above a threshold pressure), and the noble gases neon [152], argon [153] and xenon [154].

QM calculations are in general exceedingly valuable for calculating the Equation-of-State (EoS), which provides the relationship between the pressure, volume, and temperature of a given material. This information can be used to calculate a Hugoniot, which is basically the path a material traverses in the phase diagram when shocked [155,156]. Such calculations are of great utility, because of the large error bars associated in the corresponding experiments.

6 Predictions for Experiment

Theoretical calculations possess several key advantages over experiments. First, they are cheap and may be fast, especially when supercomputers are used. Second, the stoichiometry of the system under investigation may be very precisely defined, opening up the possibility of systematically studying entire phase diagrams without experimental constraints. Third, the reactivity of the material is not an issue. Fourth, the pressure range that is explored may be varied systematically without the concern of breaking diamonds, and it may exceed – quite significantly – what is experimentally attainable at this time [157]. Fifth, kinetic barriers and the lack of thermodynamic stability are not relevant since even metastable systems may be studied. In view of these features, as well as the relatively small number of groups who experimentally explore the high pressure domain, it is no surprise that there are many predictions in the literature that precede experiment. Some of these predictions have already been mentioned above [11,13,35,38,39]. Here, we provide two more examples to give the reader a flavor of computational studies preceding any experiment.

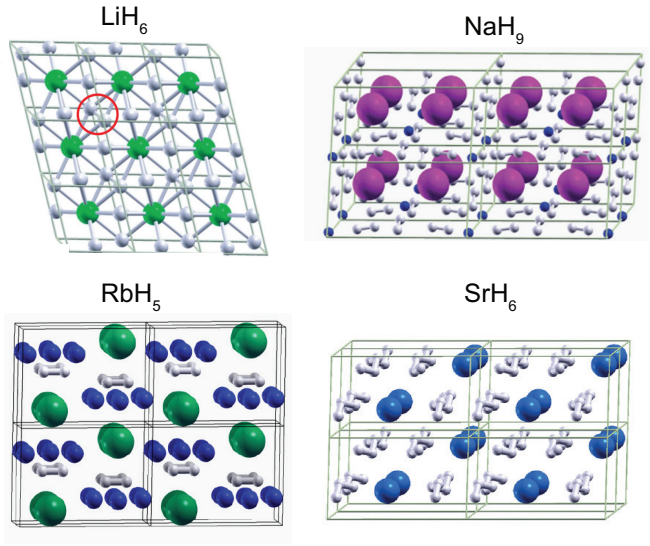

Fig. 13 Polyhydrides of an electropositive metal that are predicted to become stable under pressure. (a) LiH_6 contains $H_2^{\delta-}$ (white) [81], (b) NaH_9 contains H^- (blue) and H_2 (white) [82], (c) RbH_5 contains H_2 (white) and H_3^- (blue) [83], and (d) SrH_6 contains one dimensional helices, $^1_\infty[H^{\delta-}]$ (white) [88].

One exciting and systematically explored field is that of alkali metal and alkaline earth polyhydrides [66,81–88,158], and subhydrides [89]. The computational exploration of these phases was inspired by the proposition that doping hydrogen with the appropriate element could lead to metalization, and potential superconductivity, at experimentally achievable pressures [159]. Global optimization schemes have been employed to predict a number of phases, with non-classical stoichiometries, that become stabilized with respect to the 'classic' MH or MH_2 hydrides and H_2 at pressures ranging from 2-100 GPa. Some of these, found in the work of one of these authors (EZ), are illustrated in Fig. 13. Remarkable structural diversity is observed in the hydrogenic sublattices. They contained one or more of the following species: H_2, $H_2^{\delta-}$, H^-, H_3^-, one di-

mensional chains of $^1_\infty[H_3^-]$ or $^1_\infty[H^{\delta-}]$, and anionic atomistic cages. Phases containing $H_2^{\delta-}$ (such as LiH_6 [81,160]), atomistic polymeric chains (SrH_6 [88]) or cages (CaH_6 [66]) had the highest density of states at the Fermi level (and we are looking forward to further studies of these species using hybrid functionals, for the reasons outlined in Sec. 7). The relationship between the hydrogenic sublattices, the mechanism of metalization, and unique phonon modes that could be used as spectroscopic fingerprints to identify these structural motifs, are discussed in depth in Ref. [88]. We are looking forward to the eventual synthesis of these novel systems, and the exploration of their properties.

Another fast developing field is that of superionic conductors. The prediction that ice enters a superionic state [161] has been validated experimentally [68,162–164]. Similar predictions have been made for ammonia [161]. Moreover, full ionization of ammonia to $(NH_4^+)(NH_2^-)$ (i.e. an autoionization which is observed to a small degree in liquid anhydrous ammonia) has been predicted [51]. The latter claim has been confirmed by recent experiments [165,166]. The list of systems that have been predicted to undergo self-dissociation exceeds the class of protonic conductors. Even compounds as exotic as XeF_2, with its hypervalent F-Xe-F bonding, have been calculated to undergo transformation to the ionic XeF^+F^- polymorph at sufficiently large pressures [167]. This process is analogous to what is observed in acidic environments (for example, addition of SbF_5 Lewis acid to XeF_2 leads to the formation of XeF^+ salt), but predicted here to take place by the application of pressure alone [167].

7 Discrepancies Between Theory and Experiment

Due to the good balance between accuracy and computational expense typically provided by non-hybrid DFT calculations (of the GGA or LDA type), they are often the methods of choice for predicting structures and calculating the properties of compressed phases. But, nontrivial exchange-correlation effects can become quite important under pressure, in particular when electrons become localized (for example compressed Li [168] and Na [12,13] behave as electrides), and/or when the semicore electrons interact [169]. Moreover, standard functionals do not provide a satisfactory description of van der Waals interactions, which may be important in some compressed systems [170].

One example where non-hybrid DFT calculations were unable to predict the most stable structures observed in experiment is in the case of oxygen under pressure. Molecular oxygen is magnetic (the ground state of the O_2 molecule is a triplet), and upon solidification and further compression it undergoes a number of unique phase transformations. Around room temperature and 5.4 GPa oxygen solidifies into the non-magnetic rhombohedral β structure, which transforms into a magnetic orange δ phase at 9.6 GPa [171], followed by a red diamagnetic ε phase at 10 GPa [171], and a metallic superconducting ζ phase above 96 GPa [172–174]. It took experimentalists $\sim$30 years to determine the structure of ε-oxygen [175]. Two groups nearly simultaneously [176,177] used X-ray diffraction to show that this system is comprised of tetramers of O_2, $(O_2)_4$, which form rhombohedral molecular units that are likely held together via weak forces forming a crystal lattice with $C2/m$ symmetry consistent with the non-magnetic state of this phase.

Prior to the experimental elucidation, theory attempted to propose a structure for ε-oxygen [178,179]. First-principles calculations on geometries obtained via heuristic means illustrated that a non-magnetic system with *Cmcm* symmetry containing linear herringbone chains of O_2 molecules was the most stable in the appropriate pressure range [180]. Initial evolutionary structure searches also found this phase to have the lowest enthalpy [181], but concluded that a metastable structure better explained the experimental data available at the time [182].

Calculations illustrated that within DFT-GGA the experimentally observed ε-oxygen structure did not have the lowest enthalpy [183]. It was speculated that the discrepancy between experiment and theory could be explained by one of the following factors: a metastable phase was synthesized in the experiments, the calculations (which were carried out at 0 K) neglected temperature effects, or the exchange correlation functional was inadequate to accurately calculate relative enthalpies of different structural alternatives. Calculations on molecular models for ε-O_2 have illustrated that hybrid functionals of the B3LYP or M06 type are necessary to accurately reproduce the shape of the repulsive wall in the high-pressure regime, suggesting that non-hybrid functionals are inadequate for this system [184]. None of the functionals tested, however, were able to describe the low pressure region well [184]. In order to get a better understanding of the solid phase of ε-O_2, multireference quantum Monte Carlo calculations have been employed to study the O_4 molecule [185], and multiconfigurational *ab initio* calculations have focused on $(O_2)_4$ [186,187].

Another especially pressing problem is that of correctly predicting the onset of pressure-induced metalization of chemical elements and compounds. It is agreed that standard DFT functionals lead to a severe underestimation of electronic band gaps, and concomitantly also of metalization pressures. One approximate way to remedy this problem is by using the DFT+U method [189], which adds a Hubbard-like U term to the exchange-correlation functional for specified orbitals thereby increasing their degree of localization, and in-turn opening up a band-gap. However, U may be pressure-dependent and because of the difficulties inherent in calculating it from first-principles, U is often chosen empirically. The GW-method [190] can be used to accurately calculate the band gap of solids from

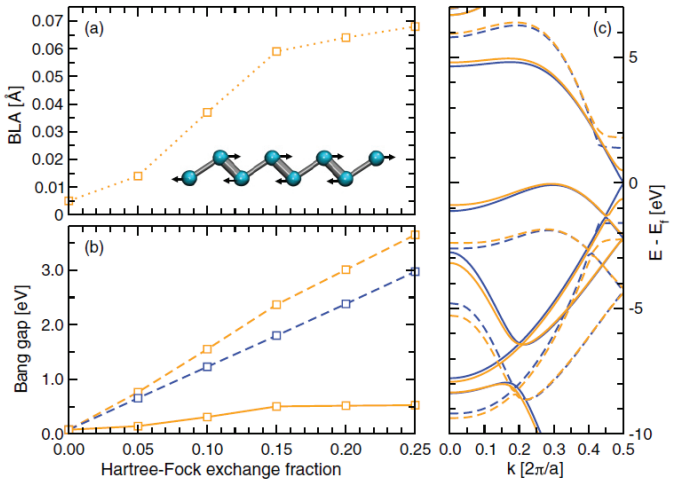

Fig. 14 (a) Bond length alternation (BLA) of a single nitrogen chain that occurs when optimized with a given amount of Hartree Fock exchange, and (b) resulting band gaps and (c) band structures. Optimization/electronic structure calculations performed with PBE/PBE (blue solid), PBE/hybrid (blue dashed), hybrid/PBE (orange solid), hybrid/hybrid (orange dashed). Note that the PBE0 functional includes 25% Hartree Fock (exact) exchange, and it is employed in (c). Reproduced with permission from Ref. [188].

first-principles, but because it is very costly it is seldom employed, a few examples can be found in Refs. [113,191]. The DFT+U approach has been used, for example, to elucidate the details of the crystal structure and electronic/magnetic band structures including the band gap for the unusual $Ag(II)SO_4$ antiferromagnet compressed up to 30 GPa [192,193], and the previously discussed LTM MOs [32].

Similarly, more sophisticated hybrid DFT and screened exchange functionals overcome many of the problems of standard LDA/GGA functionals, but they consume considerable cpu time, and their use in the community is still very limited. Therefore, diverse system for which claims have been made of their metallic and possibly superconducting properties at elevated pressures (i.e. the previously described polyhydrides whose metallicity was typically 'verified' by carrying out band structure calculations with hybrid functionals on GGA-optimized geometries [66,81–88,158]) should be carefully revisited with more accurate methods now available. In particular, small lattice distortions that lead to band gap opening should be scrutinized for all systems claimed to be metallic at certain conditions, as has been done recently for chains of nitrogen atoms [188] (see Fig. 14). In addition, it has been shown that inclusion of Hartree Fock exchange can significantly impact the calculated transition pressures between phases and demixing transitions [169,194,195].

8 Conclusions and Forecast

In this account we have presented diverse topics related to the theoretical modeling of crystalline matter subject to extreme external pressures via first-principles calculations. We have shown how modern theoretical calculations accompany experimental research by attempting to accurately reproduce experimental results, as well as describe lattice dynamics, calculate energetic and thermodynamic stability, and unveil the electronic and magnetic structure of compressed matter. We also discussed some of the most striking examples where discrepancies between theory and experiment exist. The currently available methods for structure prediction, such as data-mining, following imaginary phonons, basin/minima hopping, metadynamics, simulated annealing, random structure searches, evolutionary algorithms, the particle swarm optimization technique, and hybrid methods mixing two or more of these approaches, now enable theory to precede experiment and predict solids with interesting stoichiometries, construct entire phase diagrams, and unveil the species that might exhibit valuable physicochemical properties. A number of such successful predictions are quoted in this work.

It is not inconceivable that along with the rapid development of theoretical methods, as well as with the systematic increase of computational resources, theoreticians will have access to tools that enable them to solve certain pressing problems in the near future. For example, hybrid DFT methods – which are CPU-demanding and these days used rather scarcely – could be used for routine structure prediction. Moreover, calculations of the entire phonon spectrum for each system at every pressure point studied could become standard procedure, thus leading to the evaluation of zero-point energy corrections as well as the estimation of thermodynamic parameters; this would permit expansion of the scrutinized (p,T) field from the standard "$T = 0$ K, variable pressure" towards experimentally relevant (p,T) conditions. Accurate band gap predictions could be performed for each system, which would substantially reduce the number of claims appearing in the literature about "possibly metallic or even superconducting" properties for a given stoichiometry. Taken all together, theory might more responsibly pave the road towards new fundamental discoveries and encourage fellow experimentalists in the right direction. This progress will hopefully be associated by systematic improvement of computational methods, so that they may be able to treat correctly (and efficiently) the electronic correlation as well as long-distance electrostatic interactions in solids under conditions of extreme pressure. In addition, we forecast advances in molecular dynamics simulations and the increased use of quantum molecular dynamics [155,156,196], including electron dynamics [197], and Monte Carlo [198] studies, to further facilitate the exploration of the phase diagrams of matter beyond solid state phases. Accurate treatment of the

nuclei's quantum state[199], especially relevant for the light elements[200], may even become routine.

The types of computations we describe may lead to the discovery of new, perhaps completely unexpected, chemistry and totally new types of materials. For example, the range of the known oxidation states may be substantially expanded at high pressures by involving the semi-core electrons, such as the f-electrons of lanthanides, in chemical bonding (with the tetra-[201] and even penta- or hexavalent states probably being within reach), or sub-valence electrons of alkali metals[67]. Moreover, new exotic electronic states of matter, such as insulating gold (the ionic salt-like $Au^{+}Au^{-1}$, or gold electride, $Au^{+}e^{-}$) might possibly be created under sufficient compression. And, many other unique chemical phenomenon we have not yet imagined.

Acknowledgments

EZ acknowledges the NSF (DMR-1005413) for financial support, and thanks the Alfred P. Sloan Foundation for a research fellowship (2013-2015). WG would like to thank the Polish National Science Center (NCN) for funding (grant number 2012/06/M/ST5/00344).

Notes and references

1 W. Grochala, R. Hoffmann, J. Feng and N. W. Ashcroft, *Angew. Chem. Int. Ed.*, 2007, **46**, 3620–3642.
2 D. Machon, F. Meersman, M. C. Wilding, M. Wilson and P. F. McMillan, *Prog. Mater. Sci.*, 2014, 216–282.
3 R. Lee, J. A. K. Howard, M. R. Probert and J. W. Steed, *Chem. Soc. Rev.*, 2014, **43**, 4300–4311.
4 M. R. Manaa and L. E. Fried, *Advances in Quantum Chemistry*, 2014, vol. 69, pp. 221–252.
5 T. B. Ballaran, A. Kurnosov and D. Trots, *High Pressure Res*, 2013, 453–465.
6 A. F. Goncharov, R. T. Howie and E. Gregoryanz, *J. Low Temp. Phys.*, 2013, **39**, 402–408.
7 P. Bhardwaj and S. Singh, *Cent. Eur. J. Chem.*, 2012, **10**, 1391–1422.
8 L. Dubrovinsky and N. Dubrovinskaia, *Comprehensive Inorganic Chemistry II*, Elsevier, 2013, vol. 2, pp. 223–239.
9 D. D. Klug and Y. Yao, *Phys. Chem. Chem. Phys.*, 2011, **13**, 16999–17006.
10 M. I. Eremets, A. G. Gavriliuk, I. A. Trojan, D. A. Dzivenko and R. Boehler, *Nat. Mater.*, 2004, **3**, 558–563.
11 C. Mailhiot, L. H. Yang and A. K. McMahan, *Phys. Rev. B*, 1992, **46**, 14419–14435.
12 Y. M. Ma, M. Eremets, A. R. Oganov, Y. Xie, I. Trojan, S. Medvedev, A. O. Lyakhov, M. Valle and V. Prakapenka, *Nature*, 2009, **458**, 182–185.
13 J. B. Neaton and N. W. Ashcroft, *Phys. Rev. Lett.*, 2001, **86**, 2830–2833.
14 C. Buzea and K. Robbie, *Supercond. Sci. Technol.*, 2005, **18**, R1–R8.
15 URL http://physics.wustl.edu/∼jss/NewPeriodicTable.pdf.
16 G. Gabielse, X. Fei, L. A. Orozco, R. L. Tjoelker, J. Haas, H. Kalinowsky, T. A. Trainor and W. Kells, *Phys. Rev. Lett.*, 1990, **65**, 1317–1320.
17 R. F. Smith, J. H. Eggert, R. Jeanloz, T. S. Duffy, D. G. Braun, J. R. Patterson, R. E. Rudd, J. Biener, A. E. Lazicki, A. V. Hamza, J. Wang, T. Braun, L. X. Benedict, P. M. Celliers and G. W. Collins, *Nature*, 2014, **511**, 330–333.
18 W. Grochala, *Angew. Chem. Int. Edit.*, 2014, **53**, 3680–3683.
19 W. Zhang, A. R. Oganov, A. F. Goncharov, Q. Zhu, S. E. Boulfelfel, A. O. Lyakhov, E. Stavrou, M. Somayazulu, V. B. Prakapenka and Z. Konopkova, *Science*, 2013, **342**, 1502–1505.
20 R. Jeanloz, P. M. Celliers, G. W. Collins, J. H. Eggert, K. K. M. Lee, R. S. McWilliams, S. Brygoo and P. Loubeyre, *P. Natl. Acad. Sci. USA*, 2007, **104**, 9172–9177.
21 M. I. McMahon and R. J. Nelmes, *Chem. Soc. Rev.*, 2006, **35**, 943–963.
22 F. H. Stillinger, *Phys. Rev. E*, 1996, **59**, 48–51.
23 E. Zurek, *Reviews in Computational Chemistry*, John Wiley & Sons, Inc., Hoboken, New Jersey, accepted.
24 D. G. Pettifor, *J. Phys. C*, 1986, **19**, 285–313.
25 C. C. Fischer, K. J. Tibbetts, D. Morgan and G. Ceder, *Nat. Mater*, 2006, **5**, 641–646.
26 T. S. Bush, C. R. A. Catlow and P. D. Battle, *J. Mater. Chem.*, 1995, **5**, 1269.
27 D. M. Deaven and K. M. Ho, *Phys. Rev. Lett.*, 1995, **75**, 288–291.
28 Q. Li, Y. Ma, A. R. Oganov, H. Wang, H. Wang, Y. Xu, Y. Xu, T. Cui, H. K. Mao and G. Zou, *Phys. Rev. Lett.*, 2009, **102**, 175506 (1–4).
29 M. Amsler, J. A. Flores-Livas, L. Lehtovaara, F. Balima, S. A. Ghasemi, D. Machon, S. Pailhes, A. Willand, D. Caliste, S. Botti, A. San Miguel, S. Goedecker and M. A. L. Marques, *Phys. Rev. Lett.*, 2012, **108**, 065501 (1–4).
30 Q. Zhu, A. R. Oganov and A. O. Lyakhov, *CrystEngComm*, 2012, **14**, 3596–3601.
31 B. Meredig and C. Wolverton, *Nat. Mater.*, 2012, **12**, 123–127.
32 M. Derzsi, P. Piekarz and W. Grochala, *Phys. Rev. Lett.*, 2014, **113**, 025505.
33 D. Kurzydłowski and W. Grochala, *Acta. Phys. Polon. A*, 2011, **119**, 895–900.
34 N. W. Ashcroft, *Phys. Rev. Lett.*, 2004, **92**, 187002 (1–4).
35 J. Feng, W. Grochala, T. Jaron, R. Hoffmann, A. Bergara and N. W. Ashcroft, *Phys. Rev. Lett.*, 2006, **96**, 017006 (1–4).
36 Herein, the term "polymerization" is used to describe the process where a molecular material becomes polymeric in the sense that molecular units may no longer be recognized in its structure. Importantly, we do not refer to kinetic stability of the so-formed polymer. Indeed, some polymers may depolymerize easily, as exemplified by silane decompressed at room temperature to ambient pressure.
37 O. Degtyareva, M. M. Canales, A. Bergara, X. J. Chen, Y. Song, V. V. Struzhkin, H. Mao and R. J. Hemley, *Phys. Rev. B*, 2007, **76**, 064123 (1–4).
38 W. Grochala and D. Kurzydłowski, *NATO Science for Peace and Security Series*, Springer, 2010, pp. 357–372.
39 D. Kurzydłowski and W. Grochala, *Chem. Commun.*, 2008, 1073–1075.
40 (a) T. Söhnel, H. Hermann and P. Schwerdtfeger, *Angew. Chemie. Int. Ed.*, 2001, **40**, 4382; (b) T. Söhnel, H. Hermann and P. Schwerdtfeger, *J. Phys. Chem. B*, 2005, **109**, 526; (c) See also: R. P. Krawczyk, A. Hammerl and P. Schwerdtfeger, *ChemPhysChem*, 2006, **7**, 2286; (d) P. Schwerdtfeger, R. P. Krawczyk, A. Hammerl and R. Brown, *Inorg. Chem.*, 2004, **43**, 6707.
41 D. Kurzydłowski and W. Grochala, *Z. Annorg. Allg. Chem.*, 2008, **634**, 1082–1086.
42 (a) K. Parlinski, Z. Q. Li and Y. Kawazoe, *Phys. Rev. Lett.*, 1997, **78**, 4063. (b) K. Parlinski, Phonon Software, Kraków, 2011.
43 G. Kresse and J. Hafner, *Phys. Rev. B*, 1993, **47**, 558–561.
44 G. Kresse and J. Furthmuller, *Phys. Rev. B*, 1996, **54**, 11169–11186.
45 C. J. Pickard and R. J. Needs, *Phys. Status Solidi B*, 2009, **246**, 536–540.

46 C. J. Pickard and R. J. Needs, *J. Phys.: Condens. Matter*, 2011, **23**, 053201.

47 J. Feng, R. G. Hennig, N. W. Ashcroft and R. Hoffmann, *Nature*, 2008, **451**, 445–448.

48 C. J. Pickard and R. J. Needs, *Nat. Phys.*, 2007, **3**, 473–476.

49 Y. Yao, J. S. Tse and D. D. Klug, *Phys. Rev. Lett.*, 2009, **102**, 115503.

50 M. Marques, M. I. McMahon, E. Gregoryanz, M. Hanfland, C. L. Guillaume, C. J. Pickard, G. J. Ackland and R. J. Nelmes, *Phys. Rev. Lett.*, 2011, **106**, 095502 (1–4).

51 C. J. Pickard and R. J. Needs, *Nat. Mater.*, 2008, **7**, 775–779.

52 S. Zhang, H. Wilson, K. Driver and B. Militzer, *Phys. Rev. B.*, 2013, **87**, 024112 (1–5).

53 S. Kirkpatrick, C. D. Gelatt and M. P. Vecchi, *Science*, 1983, **220**, 671–680.

54 D. Zagorac, K. Doll, J. C. Schön and M. Jansen, *Phys. Rev. B*, 2011, **84**, 045206 (1–13).

55 A. Kulkarni, K. Doll, D. L. V. K. Prasad, J. C. Schön and M. Jansen, *Phys. Rev. B*, 2011, **84**, 172101 (1–4).

56 A. Kulkarni, K. Doll, J. C. Schön and M. Jansen, *J. Phys. Chem. B*, 2010, **114**, 15573–15581.

57 J. P. K. Doye and D. J. Wales, *J. Phys. Chem. A*, 1997, **101**, 5111–5116.

58 S. Gödecker, *J. Chem. Phys.*, 2004, **120**, 9911–9917.

59 J. A. Flores-Livas, M. Amsler, T. J. Lenosky, L. Lehtovaara, S. Botti, M. A. L. Marques and S. Goedecker, *Phys. Rev. Lett.*, 2012, **108**, 117004 (1–5).

60 T. D. Huan, M. Amsler, M. A. L. Marques, S. Botti, A. Willand and S. Goedecker, *Phys. Rev. Lett.*, 2013, **110**, 135502 (1–5).

61 A. Laio and M. Parrinello, *Proc. Natl. Acad. Sci.*, 2002, **99**, 12562–12566.

62 D. Selli, I. A. Baburin, R. Martoňak and S. Leoni, *Sci. Rep.*, 2013, **3**, 1466 (1–6).

63 J. Sun, D. D. Klug, R. Martonak, J. A. Montoya, M. S. Lee, S. Scandolo and E. Tosatti, *Proc. Natl. Acad. Sci. USA*, 2009, **106**, 6077–6081.

64 Y. Wang, J. Lv, L. Zhu and Y. Ma, *Phys. Rev. B*, 2010, **82**, 094116 (1–8).

65 Y. Wang and Y. Ma, *J. Chem. Phys.*, 2014, **140**, 040901 (1–11).

66 H. Wang, J. S. Tse, K. Tanaka, T. Iitaka and Y. Ma, *Proc. Natl. Acad. Sci. USA*, 2012, **109**, 6463–6466.

67 M. S. Miao, *Nature Chemistry*, 2013, **5**, 846–852.

68 Y. Wang, H. Liu, J. Lv, L. Zhu, H. Wang and Y. Ma, *Nat. Commun.*, 2011, **2**, 563 (1–5).

69 C. W. Glass, A. R. Oganov and N. Hansen, *Comput. Phys. Commun.*, 2006, **175**, 713–720.

70 D. C. Lonie and E. Zurek, *Comput. Phys. Commun.*, 2011, **182**, 372–387.

71 D. C. Lonie and E. Zurek, *Comput. Phys. Commun.*, 2011, **182**, 2305–2306.

72 A. R. Oganov, A. O. Lyakhov and M. Valle, *Acc. Chem. Res.*, 2011, **44**, 227–237.

73 A. N. Kolmogorov, S. Shah, E. R. Margine, A. F. Bialon, T. Hammerschmidt and R. Drautz, *Phys. Rev. Lett.*, 2010, **105**, 217003 (1–4).

74 S. Bahmann and J. Kortus, *Comput. Phys. Commun.*, 2013, **184**, 1618–1625.

75 W. W. Tipton, C. R. Bealing, K. Mathew and R. Hennig, *Phys. Rev. B*, 2013, **87**, 184114.

76 G. Trimarchi and A. Zunger, *Phys. Rev. B.*, 2007, **75**, 104113 (1–8).

77 M. d'Avezac and A. Zunger, *Phys. Rev. B.*, 2008, **78**, 064102 (1–15).

78 N. L. Abraham and M. I. J. Probert, *Phys. Rev. B.*, 2006, **73**, 224104 (1–6).

79 A. Fadda and G. Fadda, *Phys. Rev. B*, 2010, **82**, 104105 (1–8).

80 S. Q. Wu, M. Ji, C. Z. Wang, M. C. Nguyen, X. Zhao, K. Umemoto, R. M. Wentzcovitch and K. M. Ho, *J. Phys.: Condens. Matter*, 2014, **26**, 035402 (1–6).

81 E. Zurek, R. Hoffmann, N. W. Ashcroft, A. R. Oganov and A. O. Lyakhov, *Proc. Natl. Acad. Sci.*, 2009, **106**, 17640–17643.

82 P. Baettig and E. Zurek, *Phys. Rev. Lett.*, 2011, **106**, 237002 (1–4).

83 J. Hooper and E. Zurek, *Chem–Eur. J.*, 2012, **18**, 5013–5021.

84 J. Hooper and E. Zurek, *J. Phys. Chem. C*, 2012, **116**, 13322–13328.

85 A. Shamp, J. Hooper and E. Zurek, *Inorg. Chem.*, 2012, **51**, 9333–9342.

86 D. Lonie, J. Hooper, B. Altintas and E. Zurek, *Phys. Rev. B*, 2013, **87**, 054107 (1–8).

87 J. Hooper, B. Altintas, A. Shamp and E. Zurek, *J. Phys. Chem. C*, 2013, **117**, 2982–2992.

88 J. Hooper, T. Terpstra, A. Shamp and E. Zurek, *J. Phys. Chem. C*, 2014, **118**, 6433–6447.

89 J. Hooper and E. Zurek, *ChemPlusChem*, 2012, **77**, 969–972.

90 A. Hermann, N. W. Ashcroft and R. Hoffmann, *J. Chem. Phys.*, 2014, **141**, 024505.

91 A. Hermann, N. W. Ashcroft and R. Hoffmann, *Proc. Natl. Acad. Sci.*, 2012, **109**, 745–750.

92 A. Hermann, A. Suarez-Alcubilla, I. G. Gurtubay, L. M. Yang, A. Bergara, N. W. Ashcroft and R. Hoffmann, *Phys. Rev. B.*, 2012, **86**, 144110 (1–10).

93 A. Hermann, N. W. Ashcroft and R. Hoffmann, *J. Am. Chem. Soc.*, 2012, **51**, 9066–9075.

94 A. Hermann, N. W. Ashcroft and R. Hoffmann, *Chem. Eur. J.*, 2013, **19**, 4184–4197.

95 A. Hermann, A. McSorley, N. W. Ashcroft and R. Hoffmann, *J. Am. Chem. Soc.*, 2012, **134**, 18606–18618.

96 A. Hermann, B. L. Ivanov, N. W. Ashcroft and R. Hoffmann, *Phys. Rev. B*, 2012, **86**, 014104 (1–12).

97 E. Wigner and H. B. Huntington, *J. Chem. Phys.*, 1935, **3**, 764–770.

98 M. I. Eremets and I. A. Troyan, *Nat. Mater.*, 2011, **10**, 927–931.

99 R. T. Howie, C. L. Guillaume, T. Scheler, A. F. Goncharov and E. Gregoryanz, *Phys. Rev. Lett.*, 2012, **108**, 125501 (1–5).

100 C. J. Pickard, M. Martinez-Canales and R. J. Needs, *Phys. Rev. B*, 2012, **85**, 214114 (1–8).

101 See for example: M. A. Bredig, J. W. Johnson, and W. T. Smith, *J. Amer. Chem. Soc.*, 1955, **77**, 307-312, and subsequent parts of the series.

102 Triatomic molecules containing alkali metal and alkali halide are usually comproportionated: (a) W. Grochala and R. Hoffmann, *J. Phys. Chem. A*, 2000, **104**, 9740-9749; (b) W. Grochala and R. Hoffmann, *Polish J. Chem.*, 2001, **75**, 1603-1659; (c) W. Grochala, R. Hoffmann and P. P. Edwards, *Chem–Eur. J.*, 2003, **9**, 575-587. The resulting solids which contain more metal than halogen ("subhalides") are usually metallic.

103 Note, two high pressure phases, Fe_2S and Fe_3S have long been known, and both stoichiometries are far from intuitive. See also: (a) Y. W. Fei, C. M. Bertka, and L. W. Finger, *Science*, 1997, **275**, 1621-1623; (b) D. M. Sherman, *Earth Planet. Sc. Lett.*, 1995, **132**, 87-98.

104 Rotational solids and ionic conductors are two examples of systems where rotations and translations of certain sublattices are not frozen at finite temperatures and they have important contributions to the entropy.

105 N. W. Ashcroft, *Phys. Rev. Lett.*, 1968, **21**, 1748–1749.

106 C. Narayana, H. Luo, J. Orloff and A. L. Ruoff, *Nature*, 1998, **393**, 46–49.

107 P. Loubeyre, F. Occelli and R. LeToullec, *Nature*, 2002, **416**, 613–617.

108 C. J. Pickard and R. J. Needs, *Phys. Rev. Lett.*, 2006, **97**, 045504 (1–4).

109 Y. Yao, J. S. Tse, Y. Ma and K. Tanaka, *Europhys. Lett.*, 2007, **78**, 37003.

110 X. J. Chen, V. V. Struzhkin, Y. Song, A. F. Goncharov, M. Ahart, Z. Liu, H. Mao and R. J. Hemley, *Proc. Natl. Acad. Sci.*, 2008, **105**, 20–23.

111 M. I. Eremets, I. A. Trojan, S. A. Medvedev, J. S. Tse and Y. Yao, *Science*, 2008, **319**, 1506–1509.

112 X. J. Chen, J. L. Wang, V. V. Struzhkin, H. Mao, R. J. Hemley and H. Q. Lin, *Phys. Rev. Lett.*, 2008, **101**, 077002 (1–4).

113 D. Y. Kim, R. H. Scheicher, S. Lebegue, J. Prasongkit, B. Arnaud,

M. Alouani and R. Ahuja, *Proc. Natl. Acad. Sci.*, 2008, **105**, 16454–16459.
114 M. Martinez-Canales, A. R. Oganov, Y. Ma, Y. Yan, A. O. Lyakhov and A. Bergara, *Phys. Rev. Lett.*, 2009, **102**, 087005 (1–4).
115 O. Degtyareva, J. E. Proctor, C. L. Guillaume, E. Gregoryanz and M. Hanfland, *Solid State Commun.*, 2009, **149**, 1583–1586.
116 X.-F. Zhou, A. R. Oganov, X. Dong, L. Zhang, Y. Tian and H.-T. Wang, *Phys. Rev. B.*, 2011, **84**, 054543.
117 G. Gao, H. Wang, L. Zhu and Y. Ma, *J. Phys. Chem. C*, 2012, **116**, 1995–2000.
118 D. Y. Kim, R. H. Scheicher, C. J. Pickard, R. J. Needs and R. Ahuja, *Phys. Rev. Lett.*, 2011, **107**, 117002.
119 T. Scheler, O. Degtyareva, M. Marques, C. L. Guillaume, J. E. Proctor, S. Evans and E. Gregoryanz, *Phys. Rev. B.*, 2011, **83**, 214106.
120 N. Hirao, H. Fujihisa, Y. Ohishi, K. Takemura and T. Kikegawa, *Acta. Crystallogr. A*, 2008, **64**, C609–C610.
121 H. Kawamura, T. Moriwaki, Y. Akahama and K. Takemura, *Proceedings of Joint 20th AIRAPT - 43rd EHPRG International Conference on High Pressure Science and Technology*, Karlsruhe Institute of Technology, Karlsruhe, Germany, 2005, vol. 10.
122 T. Scheler, F. Peng, C. L. Guillaume, R. T. Howie, Y. Ma and E. Gregoryanz, *Phys. Rev. B*, 2013, **87**, 184117 (1–6).
123 T. A. Strobel, M. Somayazulu and R. J. Hemley, *Phys. Rev. Lett.*, 2009, **103**, 065701 (1–4).
124 P. Zaleski-Ejgierd, V. Labet, T. A. Strobel, R. Hoffmann and N. W. Ashcroft, *J. Phys.: Condens. Matter*, 2012, **24**, 155701(1–16).
125 V. Labet, R. Hoffmann and N. W. Ashcroft, *New J. Chem.*, 2011, **35**, 2349–2355.
126 E. Gregoryanz, C. Sanloup, M. Somayazulu, J. Badro, G. Fiquet, H. K. Mao and R. J. Hemley, *Nat. Mater*, 2004, **30**, 294–297.
127 B. R. Sahu and L. Kleinman, *Phys. Rev. B*, 2005, **71**, 041101 (1–3).
128 J. Uddin and G. E. Scuseria, *Phys. Rev. B*, 2005, **72**, 035101 (1–6).
129 M. B. Kanoun and S. Goumri-Said, *Phys. Rev. B*, 2005, **72**, 113103 (1–3).
130 J. C. Crowhurst, A. F. Goncharov, B. Sadigh, C. L. Evans, P. G. Morrall, J. L. Ferreira and A. J. Nelson, *Science*, 2006, **311**, 1275–1277.
131 B. R. Sahu and L. Kleinman, *Phys. Rev. B*, 2005, **72**, 119901(E).
132 J. Uddin and G. E. Scuseria, *Phys. Rev. B*, 2005, **72**, 119902(E).
133 S. K. R. Patil, S. V. Khare, B. R. Tuttle, J. K. Bording and S. Kodambaka, *Phys. Rev. B*, 2006, **73**, 104118 (1–8).
134 R. Yu and X. F. Zhang, *Appl. Phys. Lett.*, 2005, **86**, 121913 (1–4).
135 R. Yu and X. F. Zhang, *Phys. Rev. B*, 2005, **72**, 054103 (1–4).
136 R. Yu, Q. Zhan and X. F. Zhang, *Appl. Phys. Lett.*, 2006, **88**, 051913 (1–3).
137 J. von Appen, M. W. Lumey and R. Dronskowski, *Angew. Chem. Int. Ed.*, 2006, **45**, 4365–4368.
138 H. R. Soni, S. D. Gupta, S. K. Gupta and P. K. Jha, *Physica B*, 2011, **406**, 2143–2147.
139 A. F. Young, J. A. Montoya, C. Sanloup, M. Lazzeri, E. Gregoryanz and S. Scandolo, *Phys. Rev. B*, 2006, **73**, 153102 (1–4).
140 M. Wessel and R. Dronskowski, *J. Am. Chem. Soc.*, 2010, **132**, 2421–2429.
141 A. M. J. Schaeffer, W. B. Talmadge, S. R. Temple and S. Deemyad, *Phys. Rev. Lett.*, 2012, **109**, 185702 (1–5).
142 Q. J. Hong and A. van de Walle, *J. Chem. Phys.*, 2013, **139**, 094114 (1–11).
143 A. J. C. Ladd and L. V. Woodcock, *Mol. Phys.*, 1978, **36**, 611.
144 D. Alfé, G. D. Price and M. J. Gillan, *Phys. Rev. B*, 2002, **65**, 165118.
145 A. B. Belonoshko, N. V. Skorodumova, A. Rosengren and B. Johansson, *Phys. Rev. B*, 2006, **73**, 012201.
146 A. B. Belonoshko and A. Rosengren, *Phys. Rev. B*, 2012, **85**, 174104.
147 E. Sola and D. Alfé, *Phys. Rev. Lett.*, 2009, **103**, 078501 (1–4).
148 A. A. Correa, S. A. Bonev and G. Galli, *Proc. Natl. Acad. Sci. USA*, 2006, **103**, 1204–1208.
149 B. Boates, A. M. Teweldeberhan and S. A. Bonev, *Proc. Natl. Acad. Sci. USA*, 2012, **109**, 14808–14812.
150 S. A. Bonev, E. Schwegler, T. Ogitsu and G. Galli, *Nature*, 2004, **431**, 669–672.
151 J. Y. Raty, E. Schwegler and S. A. Bonev, *Nature*, 2007, **449**, 448–451.
152 M. Abbaspour and Z. Borzouie, *Fluid Phase Equilibr.*, 2014, **379**, 167–174.
153 J. Wiebke, E. Pahl and P. Schwerdtfeger, *Angew. Chem. Int. Ed.*, 2013, **52**, 13202–13205.
154 L. Shulenburger, M. P. Desjarlais and T. R. Mattsson, *Phys. Rev. B*, 2014, **90**, 140104(R).
155 L. X. Benedict, K. P. Driver, S. Hamel, B. Militzer, T. Qi, A. A. Correa, A. Saul and E. Schwegler, *Phys. Rev. B*, 2014, **89**, 224109.
156 B. Boates, S. Hamel, E. Schwegler and S. A. Bonev, *J. Chem. Phys.*, 2011, **134**, 064504.
157 J. Sun, M. Martinez-Canales, D. D. Klug, C. J. Pickard and R. J. Needs, *Phys. Rev. Lett.*, 2012, **108**, 045503 (1–5).
158 D. Zhou, X. Jin, X. Meng, G. Bao, Y. Ma, B. Liu and T. Cui, *Phys. Rev. B*, 2012, **86**, 014118 (1–7).
159 A. E. Carlsson and N. W. Ashcroft, *Phys. Rev. Lett.*, 1983, **50**, 1305–1308.
160 Y. Xie, Q. Li, A. R. Oganov and H. Wang, *Acta. Crystallogr. C*, 2014, **C70**, 104–111.
161 C. Cavazzoni, G. L. Chiarotti, S. Scandolo, E. Tosatti, M. Bernasconi and M. Parrinello, *Science*, 1999, **283**, 44–46.
162 A. F. Goncharov, N. Goldman, L. E. Fried, J. C. Crowhurst, I. F. W. Kuo, C. J. Mundy and J. M. Zaug, *Phys. Rev. Lett.*, 2005, **94**, 125508.
163 E. Sugimura, T. Komabayashi, K. Ohta, K. Hirose, Y. Ohishi and L. S. Dubrovinsky, *J. Chem. Phys.*, 2012, **137**, 194502.
164 H. F. Wilson, M. L. Wong and B. Militzer, *Phys. Rev. Lett.*, 2013, **110**, 151102.
165 T. Palasyuk, I. Troyan, M. Eremets, V. Drozd, S. Medvedev, P. Zaleski-Ejgierd, E. Magos-Palasyuk, H. Wang, S. A. Bonev, D. Dudenko and P. Naumov, *Nat. Commun.*, 2014, **5**, 3460.
166 S. Ninet, F. Datchi, P. Dumas, M. Mezouar, G. Garbarino, A. Mafety, C. J. Pickard, R. J. Needs and A. M. Saitta, *Phys. Rev. B*, 2014, **89**, 174103.
167 D. Kurzydłowski, P. Ejgierd-Zaleski, W. Grochala and R. Hoffmann, *Inorg. Chem.*, 2011, **50**, 3832–3840.
168 J. B. Neaton and N. W. Ashcroft, *Nature*, 1999, **400**, 141–144.
169 A. M. Teweldeberhan, J. L. DuBois and S. A. Bonev, *Phys. Rev. B*, 2012, **86**, 1–4.
170 B. Santra, J. Klimes, D. Alfe, A. Tkatchenko, B. Slater, A. Michaelides, R. Car and M. Scheffler, *Phys. Rev. Lett.*, 2011, **107**, 185701 (1–5).
171 M. Nicol, K. R. Hirsch and W. B. Holzapfel, *Chem. Phys. Lett.*, 1979, **68**, 49–52.
172 Y. Akahama, H. Kawamura, D. Hausermann, M. Hanfland and O. Shimomura, *Phys. Rev. Lett.*, 1995, **74**, 4690–4694.
173 S. Desgreniers, Y. K. Vohra and A. L. Ruoff, *J. Phys. Chem.*, 1990, **94**, 1117–1122.
174 K. Shimizu, K. Suhara, M. Ikumo, M. I. Eremets and K. Amaya, *Nature*, 1998, **393**, 767–769.
175 B. Militzer and R. Hemley, *Nature*, 2006, **443**, 150–151.
176 L. Lundegaard, G. Weck, M. McMahon, S. Desgreniers and P. Loubeyre, *Nature*, 2006, **443**, 201–204.
177 H. Fujihisa, Y. Akahama, H. Kawamura, Y. Ohishi, O. Shimomura, H. Yamawaki, M. Sakashita, Y. Gotoh, S. Takeya and K. Honda, *Phys. Rev. Lett.*, 2006, **97**, 085503 (1–4).
178 R. Gebauer, S. Serra, G. L. Chirotti, S. Scandolo, S. Baroni and E. Tosatti, *Phys. Rev. B*, 2000, **61**, 6145.

179 S. Serra, G. Chiarotti, S. Scandolo and E. Tosatti, *Phys. Rev. Lett.*, 1998, **80**, 5160–5163.
180 J. Neaton and N. Ashcroft, *Phys. Rev. Lett*, 2002, **88**, 205503 (1–4).
181 A. Oganov and C. Glass, *J. Chem. Phys.*, 2006, **124**, 244704 (1–16).
182 F. Gorelli, L. Ulivi, M. Santoro and R. Bini, *Phys. Rev. Lett.*, 1999, **83**, 4093–4096.
183 Y. Ma, A. Oganov and C. Glass, *Phys. Rev. B*, 2007, **76**, 064101 (1–5).
184 M. Bartolomei, J. Perez-Rios, E. Carmona-Novillo, M. Hernandez, J. Campos-Martinez and R. Hernandez-Lamoneda, *Chem. Phys. Lett.*, 2014, **592**, 170–174.
185 M. Caffarel, R. Hernandez-Lamoneda, A. Scemama and A. Ramirez-Solis, *Phys. Rev. Lett.*, 2007, **99**, 153001 (1–4).
186 M. Bartolomei, E. Carmona-Novillo, M. Hernandez, J. Perez-Rios, J. Campos-Martinez and R. Hernandez-Lamoneda, *Phys. Rev. B*, 2011, **84**, 092105 (1–4).
187 M. Garcia-Revilla, E. Francisco, A. Pendas, J. Recio, M. Bartolomei, M. Hernandez, E. Campos-Martinez, J. abd Carmona-Novillo and R. Hernandez-Lamoneda, *J. Chem. Theory Comput.*, 2013, **9**, 2179–2188.
188 B. Boates and S. A. Bonev, *Phys. Rev. B*, 2011, **83**, 174114.
189 V. I. Anisimov, J. Zaanen and O. K. Andersen, *Phys. Rev. B*, 1991, **44**, 943–954.
190 F. Aryasetiawan and O. Gunnarsson, *Rep. Prog. Phys.*, 1998, **61**, 237–312.
191 E. Kioupakis, P. Zhang, M. L. Cohen and S. G. Louie, *Phys. Rev. B*, 2008, **77**, 155114.
192 M. Derzsi, A. Budzianowski, V. V. Struzhkin, P. J. Malinowski, P. J. Leszczyński, Z. Mazej and W. Grochala, *CrystEngComm*, 2013, **15**, 192–198.
193 M. Derzsi, J. Stasiewicz and W. Grochala, *J. Mol. Model*, 2011, **17**, 2259–2264.
194 H. Liu, W. Cui and Y. Ma, *J. Chem. Phys.*, 2012, **137**, 184502.
195 B. Boates and S. A. Bonev, *Phys. Rev. Lett.*, 2013, **110**, 135504.
196 D. V. Minakov, P. R. Levashov, K. V. Khishchenko and V. E. Fortov, *J. Appl. Phys.*, 2014, **115**, 223512.
197 H. Kim, J. T. Su and W. A. Goddard III, *Proc. Natl. Acad. Sci. USA*, 2011, **108**, 15101–15105.
198 J. Chen, X. Ren, X. Z. Li, D. Alfé and E. Wang, *J. Chem. Phys.*, 2014, **141**, 024501.
199 M. A. Morales, J. M. McMahon, C. Pierleoni and D. M. Ceperley, *Phys. Rev. Lett.*, 2013, **110**, 065702.
200 J. M. McMahon, M. M. Morales, C. Pierleoni and D. M. Ceperley, *Rev. Mod. Phys.*, 2012, **84**, 1607–1653.
201 The tetravelent state is obviously rahter stable for Ce and (less so) for Tb, due to their empty and half-filled f-shells, respectively. The tetravalent state could, however, be thought of for other lanthanides, as well, and some of those could be even prone to involve even more f electrons in the chemical bonding.

Table of Contents Graphic: The role of quantum mechanical calculations for understanding and predicting the behavior of matter at extreme pressures is discussed in this feature contribution.